Highlights

Code-to-code SIMMER/FRENETIC comparison for the neutronic simulation of lead-cooled fast reactors

Mattia Massone, Nicolò Abrate, Giuseppe Francesco Nallo,
Domenico Valerio, Sandra Dulla, Piero Ravetto

- A neutronic benchmark between FRENETIC and SIMMER III/IV is presented.
- Consistent nuclear data libraries are generated with Serpent 2.
- The FRENETIC hexagonal coarse-mesh is compared to 2D cylindrical and 3D Cartesian geometrical representations in SIMMER.
- The FRENETIC nodal method diffusion solution is in very good agreement with SIMMER S_N transport solution.
- The W-ε acceleration scheme is applied to estimate the asymptotic error.

Code-to-code SIMMER/FRENETIC comparison for the neutronic simulation of lead-cooled fast reactors

Mattia Massone[a], Nicolò Abrate[b], Giuseppe Francesco Nallo[b], Domenico Valerio[b], Sandra Dulla[b], Piero Ravetto[b]

[a] *Karlsruher Institut für Technologie - Institut für Neutronenphysik und Reaktortechnik, Hermann-von-Helmholtz-Platz 1, 76344 Eggenstein-Leopoldshafen (Germany)*
[b] *Politecnico di Torino, Dipartimento Energia, Corso Duca degli Abruzzi, 24 - 10129 Torino (Italy)*

Abstract

This paper presents a neutronic benchmark between the FRENETIC and the SIMMER codes, performed considering the core of the ALFRED lead-cooled fast reactor. FRENETIC includes a nodal diffusion module developed for fast full-core analyses of safety-relevant transients in liquid-metal fast reactors, while SIMMER is a reference tool for qualifying such kind of systems in accidental conditions. In order to highlight the influence of the different numerical methods available in the two codes on the output responses, macroscopic parameters like the effective multiplication factor and the linear power are compared in an increasingly detailed simulation framework. The 3D full-core FRENETIC results are compared at first to a cylindrical 2D SIMMER core model, to highlight the impact of the absorber rings location. Then, a 3D full-core model is also employed in SIMMER to assess the differences, with respect to FRENETIC, induced by the adoption of a Cartesian mesh and of the discrete ordinates method. The full input data consistency is ensured providing the same set of few-group material constants, generated with the Monte Carlo code Serpent 2. Finally, the W-ε scheme is applied to accelerate the angular and spatial convergence of the k_{eff} sequences computed by SIMMER in order to estimate the asymptotic errors with respect to the

Email addresses: mattia.massone@kit.edu (Mattia Massone), nicolo.abrate@polito.it (Nicolò Abrate), giuseppefrancesco.nallo@polito.it (Giuseppe Francesco Nallo), domenico.valerio@polito.it (Domenico Valerio), sandra.dulla@polito.it (Sandra Dulla), piero.ravetto@polito.it (Piero Ravetto)

reference Serpent calculation.

Keywords: SIMMER, Serpent, FRENETIC, neutronic benchmark, ALFRED, Lead-Cooled Fast Reactors, control rod models, 2D cylindrical model, W-ε acceleration

1. Introduction

The Lead-cooled Fast Reactor (LFR) is one of the most promising Generation IV concepts. Its main objectives are the minimization of long-lived radioactive waste, the economic sustainability and the inherent safety. Safety aspects have to be incorporated early in the design phase to ensure compliance with the above-mentioned objectives. Due to the different characteristics of LFRs with respect to thermal reactors, codes commonly employed for the accidental analysis in LWRs may not be adequate. Therefore, there is a need for *ad hoc* computational tools that could accurately catch all the physical details occurring during both the reactor operational and off-operational states.

In this perspective, the Fast REactor NEutronics/Thermal-hydraulICs (FRENETIC) code, a multiphysics tool for the full-core analysis of liquid metal-cooled reactors with hexagonal sub-assemblies (SAs), has been developed at Politecnico di Torino in the framework of the research and development activities associated to the Advanced Lead-cooled Fast Reactor European Demonstrator (ALFRED) design. FRENETIC includes a neutronic and a thermal-hydraulics module, which have been already validated against experimental data (Caron et al., 2018) and benchmarked with reference codes (Zanino et al., 2014).

Recently, the neutronic module has been further benchmarked (Nallo et al., 2020) with respect to the Serpent 2 Monte Carlo code (Leppänen et al., 2015), showing fairly good results in terms of the assembly-wise power distribution and the effective multiplication factor. That previous work showed how the inclusion of some inactive regions, e.g. the core barrel, in the reactor model is of paramount importance for the accurate evaluation of the main neutronics quantities. That paper also assessed the very good agreement between the thermal feedback effects evaluated by FRENETIC, which relies on a library of pre-computed, temperature-dependent few-group constants, and Serpent, which directly adjusts the continuous-energy nuclear data. However,

the impact of the different numerical and modelling approximations present in FRENETIC (e.g. the nodal diffusion instead of a mesh-less transport model) on the final results was not studied in detail.

The estimation of the different contributions to the approximation error would be fundamental for assessing the Predictive Capability Maturity Model (PCMM) (Oberkampf et al., 2007) of FRENETIC. However, the discretisation-free nature of the Monte Carlo approach does not allow to clearly distinguish between the different spatial, angular and energy approximations using Serpent as a reference tool. For this reason, in the present paper FRENETIC is benchmarked with SIMMER III/IV (Kondo et al., 2000), which is a reference multiphysics tool in the context of core-disruptive accidents in liquid metal-cooled fast reactors (Maschek et al., 2008). The features of the neutronic module of SIMMER, a multi-group discrete ordinates code, fit well the FRENETIC qualification needs, allowing to develop a progressively detailed simulation framework, with the objective of assessing and isolating the different discrepancies between the two tools.

After a presentation of the main features of the codes employed and of the system under study, i.e. the ALFRED design developed in the European research project LEADER (Grasso et al., 2014), the present paper focuses first on the geometrical modelling effects: SIMMER allows to construct 2D axially symmetric and 3D core models, approximating the hexagonal SAs with a cartesian mesh, while FRENETIC represents exactly the SAs, but with a 3D model only. Then, the effects of the angular variable treatment - diffusion in FRENETIC against S_N in SIMMER - is assessed. The code-to-code comparison is focused on the main output parameters of practical interest, namely the effective multiplication constant k_{eff}, the assembly-wise fission power and the multi-group neutron flux. To ensure the full consistency of the code-to-code comparison, the very same set of homogenised few-groups data, computed with Serpent, is employed in both codes. Finally, some conclusions are drawn and future perspectives concerning the optimization of the energy discretisation by means of a genetic algorithm (Massone et al., 2017) are discussed.

2. Computational tools

In this section, the main features of the codes used throughout the paper are presented.

2.1. The FRENETIC code

The FRENETIC purpose is the multiphysics (neutronic and thermal-hydraulic) simulation of the steady-state and transient behaviour of the full core of liquid metal-cooled fast reactors adopting hexagonal, closed sub-assemblies (Bonifetto et al., 2013). Specifically, FRENETIC was designed to allow for the fast and efficient simulation of operational and off-operational core transients, in support of both the design and the verification phases. For this reason, the code does not aim at resolving the neutronic problem up to the pin level nor the thermal-hydraulic problem up to the sub-channel level, but rather it focuses on the sub-assembly scale. In this way, by adopting simplified physical models, FRENETIC allows to simulate several full-core configurations in short time, with the inclusion of the feedback related to power, temperature or modifications to the core configuration.

The code is composed of two separate neutronics (NE) and thermal-hydraulics (TH) modules, which communicate exchanging the power (NE to TH) and the temperatures (TH to NE) at each time-step. The TH module solves the 1D conservation equations for the coolant along each closed SA, accounting for the inter-assembly thermal coupling, and includes a 1D radial model for the fuel pin, locally coupled to the coolant; the NE module computes the neutron flux and power distribution with an *ad hoc* nodal method for the time-dependent multi-group diffusion equations (Caron et al., 2016). A coarse-mesh approach is employed to discretise the computational domain, and the flux is integrated in each sub-volume to get the thermal power distribution for the TH. The modules of the FRENETIC code have been validated against other computational tools and against experimental data both in stand-alone configuration (Zanino et al., 2012, 2014), and in coupled calculations, as for the EBR-II SHRT-45R test in the frame of a Coordinated Research Project of the International Atomic Energy Agency (Caron et al., 2018).

2.2. The SIMMER code

SIMMER is a multi-dimensional, multi-velocity field, multiphase, multicomponent, Eulerian, fluid dynamics code coupled with a space and energy dependent neutron kinetics module and a structure model (Bohl and Luck, 1990; Yamano et al., 2008; Tobita et al., 2006a; Kondo et al., 2000), developed by JNC (Japan Nuclear Cycle Development Institute) in cooperation with KIT (Karlsruhe Institute of Technology), CEA (Commissariat à

l'énergie atomique et aux énergies alternatives), IRSN (Institut de radioprotection et de sûrete nucléaire) and many other international research centres and universities. SIMMER was primarily developed for studying LFRs in core disruptive accident scenarios (Tobita et al., 2006b) but, given its flexibility, it can be employed in a much wider range of applications, including light water reactors, molten salt reactors (Wang et al., 2006), Accelerator Driven Systems and general multiphase problems (Kondo et al., 2000). The neutronic solver, originally based on the static code DANTSYS (Alcouffe et al., 1995), employs standard finite-difference techniques for the solution of the multi-group discrete-ordinates transport equation (Bohl and Luck, 1990); the macroscopic cross-sections are calculated based on the isotopic composition of homogeneous cells, corrected for resonance self-shielding following the Bondarenko method (Bondarenko, 1964). The flux distribution provided by the neutronic section is transferred at each time-step to the fluid dynamics and the structure modules, which use it to assess the temperature distribution and the effects on the structural integrity; structure disintegration and material movement within the system is also taken into account in order to correctly model the accidental behaviour. This results in cells isotopic composition and temperature evolving along the calculation, which constitute the thermal-hydraulic and structure modules feedbacks to the neutronic solver for the recalculation of the macroscopic cross-sections.

3. Code-to-code comparison simulation framework

This section presents the simulation setup employed for the code-to-code comparison.

3.1. Input data consistency

Since the aim of this work is to assess the impact of the different numerical and modelling approaches employed in the neutronic model of the two codes, it is of paramount importance to guarantee that their models and input data are as consistent as possible. One important difference between the two codes concerns the multi-group cross-section library management. FRENETIC needs a set of few-group parameters for each region specified by the user, while SIMMER usually computes internally the multi-group cross-section set needed for the full-core calculation based on the actual core condition. To eliminate this source of discrepancy, the SIMMER code input data reader has been extended to accept as input the homogenised data as

read by FRENETIC, i.e. a HDF (Hierarchical Data Format) file. The main advantages of this format are its standardization, which allows to read the file with the main programming languages, its hierarchical structure, which naturally allows to organise the multi-group data for each region in a systematic way, and the possibility to add metadata to enhance data usability (Folk et al., 2011). This procedure is implemented with a suitable set of Python classes that exploit the serpentTools package (Johnson et al., 2020) to parse the Serpent output and then write the few-group constants into the HDF file.

3.2. ALFRED core geometrical model

Another difference among the two codes concerns the treatment of the core geometry. FRENETIC allows to consider 2D systems, where the reactor is assumed to be constituted by flat, hexagonal SAs, or three-dimensional systems, where each SA is axially extruded. In this last case, the z-axis is discretised in bins, while the hexagonal shape of the SAs is considered in the specific implementation of the nodal method, both in 2D and 3D. Conversely, SIMMER allows to treat the full core with a detailed three-dimensional cartesian discretisation, or to reduce the geometrical complexity by means of a cylindrical r-z discretisation, thus preventing to identify the polar localization of specific assemblies, such as the Control Rods (CRs). These differences

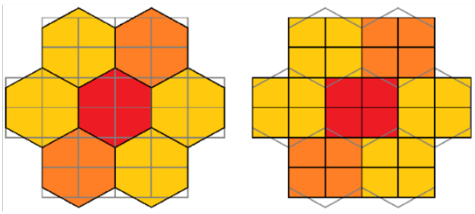

Figure 1: Cartesian mesh employed by SIMMER to approximate the hexagonal geometry.

in the geometrical model have suggested to compare the FRENETIC 3D calculations with both the 2D and 3D SIMMER models, in order to estimate the influence of the cartesian approximation of the hexagons, whose shape is slightly perturbed as sketched in Figure 1, and the impact of the position of the CR rings in the cylindrical model. In this last case, an *ad hoc* ALFRED model without safety and control rods is also employed in order to obtain a

3D core as close as possible to the axisymmetric cylinder. For the sake of conciseness, the comparison between the cylindrical SIMMER and the 3D FRENETIC models are presented in Appendix A.

3.3. Few-group constants generation

The few-group constants employed for the full-core calculations have been computed using the Serpent 2 continuous-energy Monte Carlo code (Leppänen et al., 2015), which is one of the reference tools employed to homogenise in space and to collapse in energy the nuclear data needed for deterministic codes.

The 3D ALFRED core model employed for the Serpent calculations in this work is the same as in (Nallo et al., 2020), i.e. the design produced in the LEADER project (Grasso et al., 2014) at Beginning of Cycle (BoC) and at the uniform temperature of 673 K. The different sub-assemblies (fuel, control, dummy and so on) are represented with a pin-by-pin heterogeneous model, while the barrel and the reflectors are assumed to be made of homogeneous materials.

Using this Serpent model, different axial and radial subdivisions are employed in Serpent for the nuclear data homogenisation, while the same six-group grid employed in (Nallo et al., 2020) and reported in Table 1 is used for the energy collapsing. Concerning the nuclear data library, the more recent ENDF-B/VIII.0 library (Brown et al., 2018) is adopted here instead of the JEFF-3.1 employed in the reference paper. The Serpent criticality calculation yields a k_{eff} equal to 1.08122(3)[1] with JEFF-3.1 and equal to 1.07616(4) with the ENDF-B/VIII.0, meaning that the choice of the library has a strong impact ($\sim$ 500 pcm) on the final output. The Serpent model is used in two configurations: in the first one, indicated in the following as *off-critical*, the CRs are completely withdrawn; in the second one, the CRs are inserted in such a way that the upper edge of the absorber zone is 11 cm above the core midplane, which is located at the half-height of the fuel assemblies active zone. This configuration, indicated in the following as *close-to-critical*, allows to almost achieve criticality (k_{eff}=1.00002(4)). It should be noticed that, for the specific reactor design here considered, the CRs are inserted from below.

[1] In the following, the number in parentheses denotes the standard deviation, in terms of 1σ with respect to the last digit before the parentheses.

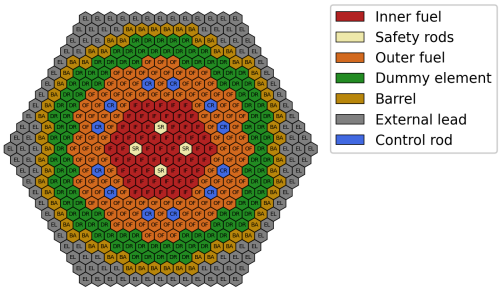

Figure 2: Radial (x-y plane) section of the ALFRED 3D model for the few-group constants calculation.

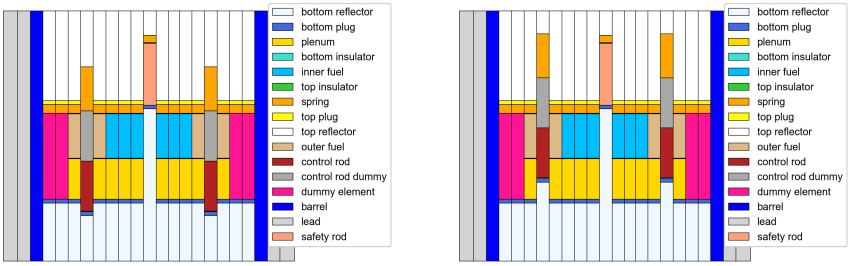

Figure 3: Off-critical (left) and close-to-critical (right) axial (x-z plane) configurations of the ALFRED 3D model for the few-group constants calculation.

Hereafter, the term *region subdivision* will refer to the core radial and axial regions employed for the few-group data homogenisation and collapsing performed in Serpent, whilst the term *partition* will refer to the planes, parallel to the z-axis, adopted to define the axial regions employed in the deterministic core model. As mentioned above, two different subdivisions are considered for the spatial homogenization of the nuclear data. The first subdivision, visible in Figure 2 (left) radially and in Figure 3 (right) axially, follows the reference (Nallo et al., 2020). The axial subdivision tries to accurately represent the different core regions, yielding one set of data for each component, e.g. the plug, spring and insulator. Figure 3 (right) indicates that the CRs absorber regions are inserted; actually, the few-group data for this configuration are generated with the off-critical Serpent model, see Figure 3 (left). For the sake of conciseness, this version will be henceforth indicated as *version A*. The second subdivision, depicted in Figure 4, distinguishes radially among a larger number of different regions, but is axially less detailed. The rationale for this choice consists in increasing the

radial detail of the data at the expense of the axial homogenisation of some optically thin structural regions, e.g. the plugs and insulators, which are spatially homogenised with the reflector. The few-group data for such configuration, indicated in the following as *version B*, are generated with the close-to-critical Serpent configuration. The data for version A are generated using 100 inactive and 200 active cycles with 10^6 particles each, which proved to yield a satisfactory statistical convergence. Conversely, the data for version B are computed using 200 inactive and 300 active cycles with 10^6 particles each, which provided unnecessarily low statistical noise. These different settings led to different computational burdens, roughly scaled according to the number of neutron histories. Clearly, it would be possible to reduce the cost associated to the data generation of version B, thus further justifying its adoption with respect to version A.

Table 1: Six-group energy grid adopted to perform the macroscopic cross section energy collapsing as in (Nallo et al., 2020).

Group	Upper boundary (MeV)	Lower boundary (MeV)
1	$2.000 \cdot 10^{1}$	$1.353 \cdot 10^{0}$
2	$1.353 \cdot 10^{0}$	$1.832 \cdot 10^{-1}$
3	$1.832 \cdot 10^{-1}$	$6.738 \cdot 10^{-2}$
4	$6.738 \cdot 10^{-2}$	$9.119 \cdot 10^{-3}$
5	$9.119 \cdot 10^{-3}$	$2.000 \cdot 10^{-5}$
6	$2.000 \cdot 10^{-5}$	$1.000 \cdot 10^{-11}$

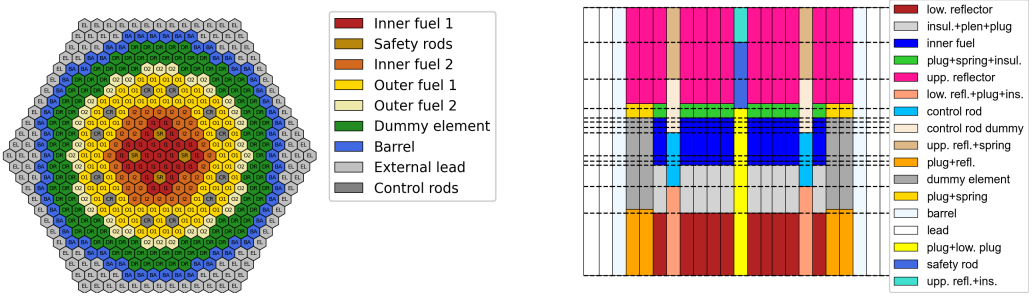

Figure 4: Radial (left) and axial (right) sections of the ALFRED 3D model for the few-group constants calculation, version B.

4. Numerical results

In this section, the main numerical results obtained from the code-to-code comparison are presented and discussed, in order to get a better insight of the various approximation errors.

4.1. Sensitivity study on axial region partition and geometry effects

The dashed, black lines appearing in Figure 4 (and Figures A.14 and A.15 in Appendix A) indicate the above-mentioned *partitions* used in the deterministic codes. Indeed, contrarily to Serpent, both FRENETIC and SIMMER require each axial plane to extend over the whole reactor, leading to partitions possibly encompassing several of the axial subdivisions adopted in Serpent. In both deterministic codes, each axial partition is then typically further sliced into *sub-partitions* to appropriately solve the discretised equations. Nuclear data within each partition are homogenised *a posteriori* in order to avoid optically thin regions that could jeopardize the convergence of the nodal diffusion method (Marchetti, 2017). According to this strategy, it may occur that different subdivisions, i.e. some regions, are merged into a unique volume, introducing local distortions in the spectrum and in the spatial distribution in addition to the numerical ones. As visible in Figure 5, the

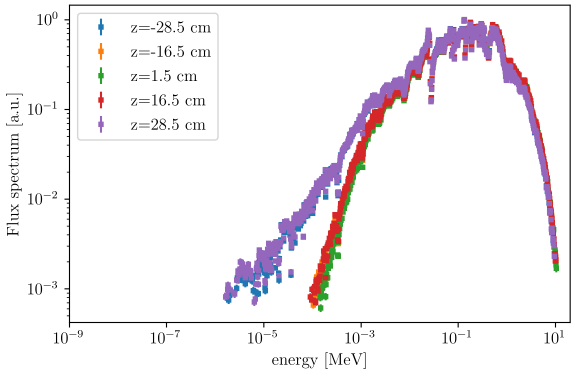

Figure 5: Axial behaviour of the neutron flux spectrum in the fuel, computed by Serpent.

flux energy spectrum computed by Serpent shows a non-negligible gradient from the active length edge to the its center, implying possible significant variations in the collapsed few-group data.

A sensitivity study was first performed on the axial regions subdivision and partition, comparing the 2D SIMMER results and the 3D FRENETIC ones. The results, reported in Appendix A, suggest that the 2D model is too simple to draw a fair comparison with both FRENETIC and Serpent, due the strong effects related to the cylindrical shape and to the presence of the neutron absorber rings. The outcomes of this analysis also suggest that, in order to approach the reference k_{eff}, more axial regions are needed to reproduce more accurately the spectrum gradient in the active height. Conversely, it seems that the peripheral axial regions have an almost negligible impact on the calculation accuracy. In the light of these considerations, the following section presents an analysis of the 3D calculations performed by SIMMER and FRENETIC using the data generated with ALFRED B model, which aims at incorporating the outcomes discussed above with a more detailed region subdivision.

4.2. 3D code-to-code benchmark

The next step in the benchmark activity consists in the comparison of SIMMER and FRENETIC for the same 3D ALFRED B model, sketched in Figure 4, in terms of k_{eff}, assembly-wise power distribution and linear power in two representative FAs.

4.2.1. Results for the close-to-critical configuration

Several S_N discretization orders have been considered in SIMMER. The compositions along the SAs have been represented consistently between the two codes, following the procedure described in (Nallo et al., 2020). In Table 2, the values of k_{eff} for each SIMMER S_N order are compared with the ones calculated by FRENETIC and Serpent; as done in the previous sections, the latter is taken as reference. The S_2 case, in Figure 6, shows rather large discrepancies in both power and axial distributions; these differences are evident also looking at the k_{eff}, which differs from Serpent and FRENETIC by more than 180 pcm. The power distribution discrepancies are affected by the Cartesian-hexagonal mesh approximation, which might play a particular role in combination with the limited number of directions available for the streaming.

Excluding the S_2 case, whose behaviour has been already commented, SIMMER seems to show the tendency to converge to a k_{eff} lying between Serpent and FRENETIC when the S_N order increases. Such behavior is

expected, since the cross-sections computed by Serpent have been post-homogenised and therefore SIMMER should not converge to the Serpent value. Notwithstanding this, SIMMER provides better results than FRENETIC, considering that the solution scheme is based on transport rather than diffusion. In general, calculations from S_4 to S_8 provide very similar results, with excellent agreement in terms of both power and linear distributions. The differences are concentrated in the neighbourhood of the CRs (with the worst behavior observed for cells which are near two CRs), as expected with diffusion codes. The effect of the Cartesian-hexagonal mesh difference is clear in all cases, as the results do not show the 60° symmetry that is proper of the design. A closer look to Figure 7, compared with Figures 8 and 9, shows that the S_4 case provides slightly lower discrepancies between SIMMER and FRENETIC. This does not mean that the SIMMER S_4 better represents the physics, rather that it is closer to the description produced by the FRENETIC diffusion calculation. Actually, the S_4 case is already an adequate description of the core physics, as opposed to the S_2 scenario.

Table 2: Comparison among k_{eff} provided by SIMMER (SMR) at different S_N order, and k_{eff} computed with FRENETIC (FRN) and Serpent (SRP). The reference case is provided by Serpent, $k_{\text{eff,SRP}} = 0.99999(8)$, whereas FRENETIC yields $k_{\text{eff,FRN}} = 0.99819$ ($\Delta k_{\text{eff,SRP-FRN}}$=172 pcm).

	S_2	S_4	S_6	S_8
$k_{\text{eff,SMR}}$	0.99631	0.99973	0.99927	0.99908
$k_{\text{eff,SMR}} - k_{\text{eff,FRN}}$ [pcm]	-188.57	154.79	108.74	89.71
$k_{\text{eff,SMR}} - k_{\text{eff,SRP}}$ [pcm]	-368.97	-25.61	-71.65	-90.68

Table 3: Comparison among k_{eff} computed by FRENETIC, SIMMER and Serpent for the configurations with CRs withdrawn and inserted.

	FRENETIC	SIMMER (3D, S_8)	Serpent
$k_{\text{eff,CR}_{\text{out}}}$	1.07924	1.08256	1.07616(4)
$k_{\text{eff,CR}_{\text{in}}}$	0.99818	0.99973	0.99999(8)
CR worth [pcm]	8106	8283	7616(9)

4.2.2. Results for the off-critical configuration

In order to assess the effect of the CRs on the flux and power profiles commented before, an additional case with the CRs extracted from the active

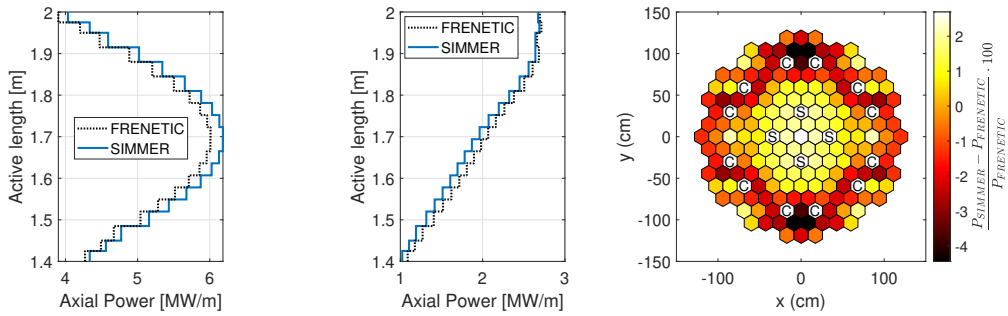

Figure 6: Relative difference on the assembly-wise power (right) and axial power profiles (left and centre) for the S_2 case. The left axial profiles correspond to the central FA; the centred ones, to the FA between two CRs in the 2^{nd} sextant.

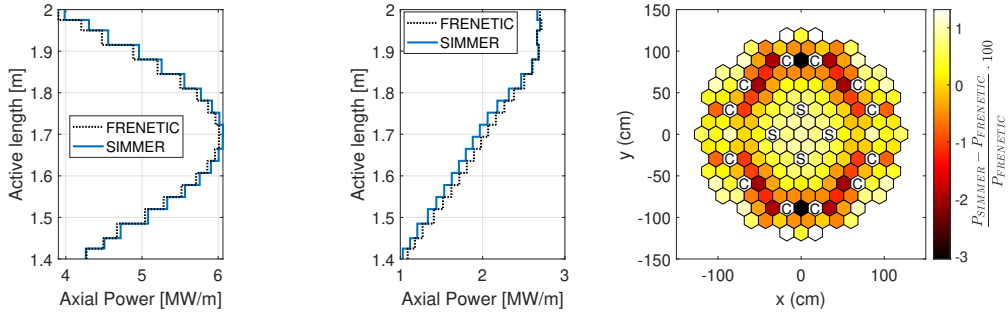

Figure 7: Relative difference on the assembly-wise power (right) and axial power profiles (left and centre) for the S_4 case. The left axial profiles correspond to the central FA; the centred ones, to the FA between two CRs in the 2^{nd} sextant.

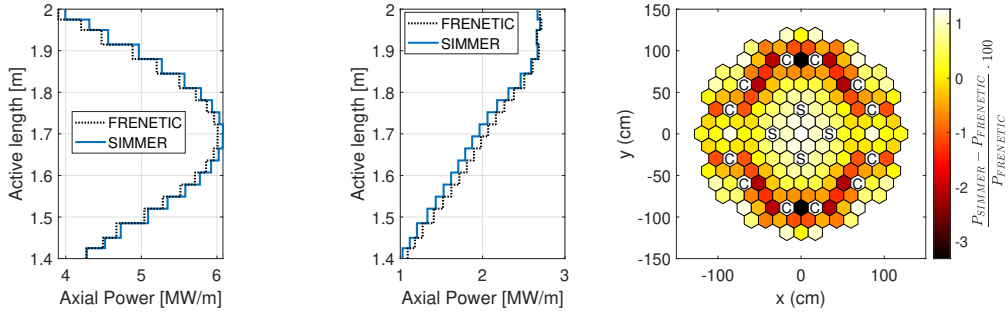

Figure 8: Relative difference on the assembly-wise power (right) and axial power profiles (left and centre) for the S_6 case. The left axial profiles correspond to the central FA; the centred ones, to the FA between two CRs in the 2^{nd} sextant.

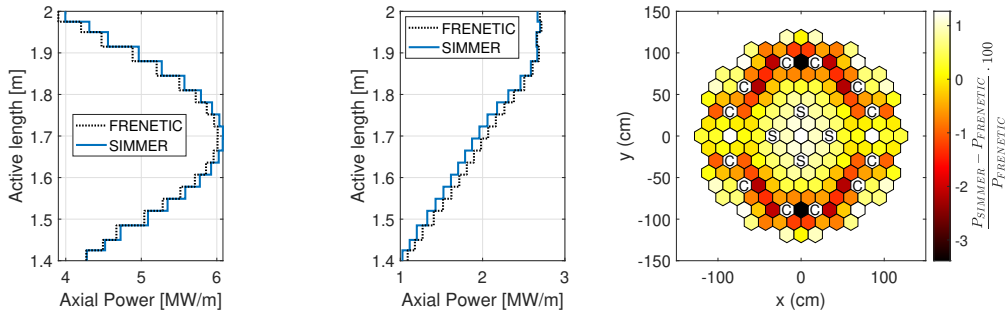

Figure 9: Relative difference on the assembly-wise power (right) and axial power profiles (left and centre) for the S_8 case. The left axial profiles correspond to the central FA; the centred ones, to the FA between two CRs in the 2^{nd} sextant.

region has been studied.

Table 3 provides the multiplication factor differences calculated by FRENETIC, SIMMER and Serpent, and hence the worth of the CR bank. SIMMER and FRENETIC are in very good agreement, predicting a CR worth that differ by just 2 %. This agreement is evident also from Figure 10, showing that the CR effect on the power per FA predicted by the two codes correspond in most of the positions. The largest discrepancies are observed in the neighbourhoods of the CRs, which is in line with poor representation offered by the diffusion in presence of absorbers.

In fact, diffusion fails to adequately model large anisotropies: indeed, the presence of CRs causes a large distortion in the flux - and, hence, in the power - for neighbouring FAs, both radially and axially. The central plots in Figure 6 to Figure 9, representing all the S_N simulations, show that the results of the two codes tend to be very different at the bottom, while the profiles agreement improves with the elevation, where the absorber effect is less significant. Considering that the CRs are inserted from the bottom, this observation is in line with the expectations, in that diffusion, as opposed to transport, is not able to correctly model the flux in the vicinity of strongly absorbing materials. This fact, together with the already commented difference in the Cartesian-hexagonal modelling adopted by the codes, produces the evident difference in the radial power map in Figure 9. Therefore, the power distributions of the case having the CR extracted (Figure 11) presents much lower discrepancies than the corresponding case with the CRs inserted (Figure 9).

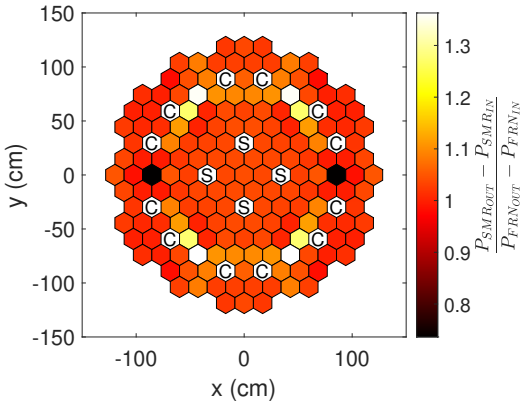

Figure 10: Ratio between the power differences calculated by SIMMER and the power differences computed by FRENETIC when the CRs are withdrawn/inserted. The 3D ALFRED B model is adopted for the simulation for both FRENETIC and SIMMER (S_8) employing the same number of axial nodes.

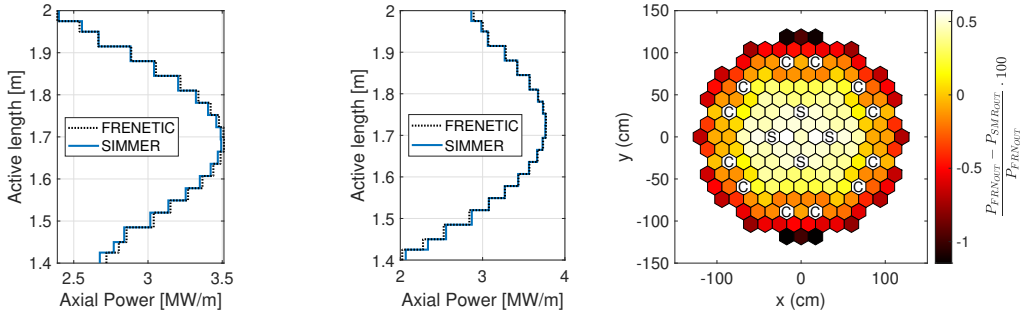

Figure 11: Relative difference on the assembly-wise power (right) and axial power profiles (left and centre) for the S_8 case with extracted CR configuration. The left axial profiles correspond to the central FA; the centred ones, to the FA between two CRs in the 2^{nd} sextant.

4.3. Spatial and angular convergence acceleration

In this section, the W-ε scheme (Wynn, 1956; Ganapol, 2014) is employed to extrapolate the SIMMER results to the different approximations limits, accelerating the convergence of k_{eff} sequences in space and angle. This algorithm, which belongs to a wider class of methods based on the Shanks transformation (Shanks, 1955), is a non-linear scheme that allows to estimate the asymptotic limit of a finite sequence. In this work, the accelerations are performed using the mpmath python package (Fredrik Johansson, 2017).

The objective of this section is to estimate the behaviour of the spatial and angular approximation errors in FRENETIC with respect to the most accurate available SIMMER results. As mentioned previously, one of the main advantages of using SIMMER instead of a continuous-energy Monte Carlo code like Serpent lies in the fact that it allows to use the same FRENETIC few-group input data varying the spatial and angular resolution. Thanks to this feature, it is possible to construct sequences characterised by increasing accuracy that could be accelerated in space, in angle or both. As recently shown in (Abrate et al., 2021a) for a simple plane geometry system, the double acceleration is crucial to minimise the bias induced by the spatial and angular approximations and to get a converged solution that is very close to the reference value, when available.

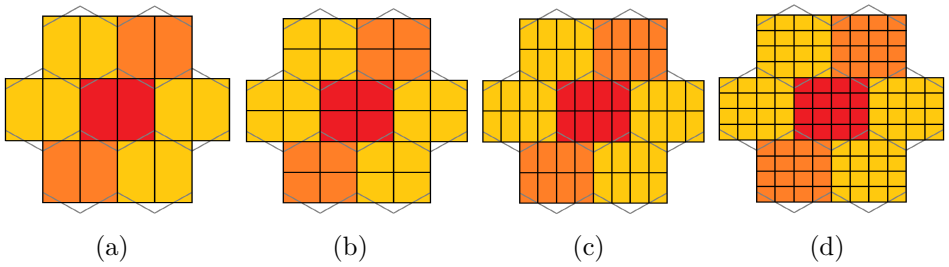

Figure 12: Progressive refinement of the x-y SIMMER meshing from the coarsest (a) to the finest (d)

Following this approach, a set of 64 eigenvalues is computed with SIMMER combining four different Cartesian meshes with four axial discretisations for each of the even discrete ordinates orders ranging from 2 to 8. The meshes on the x-y plane and the nodes along the z axis will be labelled in the following as r and z, respectively, followed by a number from 1, i.e. the coarsest, to 4, i.e. the finest.

N	r_4, z_4	W-$\varepsilon(r)$, z_4	W-$\varepsilon(z)$, r_4	W-$\varepsilon(r, z)$	W-$\varepsilon(z, r)$
2	284(8)	324(8)	262(8)	190(8)	161(8)
4	-35(8)	-8(8)	-89(8)	-81(8)	-88(6)
6	-7(8)	33(8)	-42(8)	0(8)	0(8)
8	2(8)	44(8)	6(8)	-33(8)	-35(8)
W-$\varepsilon(r, z,$ N)			-19(8)		
W-$\varepsilon(z, r,$ N)			-23(8)		

Table 4: Distance between the reference $k_{\text{eff,SRP}}$=0.9999(8) and the effective multiplication factor computed by SIMMER and accelerated with the W-ε scheme for the different discrete ordinates order.

As described in Figure 1, the Cartesian horizontal mesh is subdivided into rectangles: the coarsest geometry considers 2 meshes per rectangle; with each refinement, each rectangle is further halved (Figure 12). The axial subdivision is chosen aiming at meshes of about 20 cm, 10 cm, 7.5 cm or 5 cm height, as refinement increases; it must be anyhow be noticed that the axial submesh has to match with the macroscopic cross-section main meshing, hence the actual height of the cells might differ from the considered dz.

To appreciate the impact of the single SIMMER approximations, i.e. axial, radial or angular, the acceleration is applied to two variables at a time, thus reducing as much as possible their contribution to the overall error. Contrarily to (Abrate et al., 2021a), where the extrapolations are performed with a large dataset (∼500-1000), the amount of data used in this work is quite limited, due to the computational burden required. Hence, more attention will be focused on the general acceleration trend rather than on the final extrapolations, which could improve if more data were employed.

Tables 4 to 6 compare the reference k_{eff} for the close-to-critical configuration, computed by Serpent, with the accelerated sequences computed by SIMMER, while the same residuals computed with respect to FRENETIC are reported in Appendix B, see Tables B.11 to B.13. Each table focuses on the acceleration of each possible couple out of the three discretised variables, i.e. the discrete ordinates order N, r and z. The first column of these tables provides the non-accelerated k_{eff} values computed with the finest approximations for each value of the third parameter, which will be addressed as *frozen*

z	r_4, S_8	W-$\varepsilon(r)$, S_8	W-ε(N), r_4	W-$\varepsilon(r$, N)	W-ε(N, r)
1	226(8)	281(8)	208(8)	261(8)	261(8)
2	87(8)	139(8)	74(8)	123(8)	123(8)
3	36(8)	61(8)	10(8)	55(8)	55(8)
4	2(8)	44(8)	-9(8)	28(8)	28(8)
W-$\varepsilon(r$, N, $z)$			-11(8)		
W-ε(N, r, $z)$			-11(8)		

Table 5: Distance between the reference $k_{\text{eff,SRP}}$=0.9999(8) and the effective multiplication factor computed by SIMMER and accelerated with the W-ε scheme for each axial discretisation.

parameter in the following, to show their distance from the reference. The second and third columns show the effect of accelerating only one of the two variables, while the last ones report the results of the double accelerations performed exchanging the order of the two variables in the W-ε scheme, in order to assess whether there are strong effects due to the non-linearities in the acceleration scheme. For the same reason, each table shows the results of the accelerations involving all the dispositions obtained from the three parameters. The notation W-$\varepsilon(x)$ in the tables means applying the Wynn-epsilon scheme to a sequence with x as a varying parameter, while W-$\varepsilon(x, y)$ means that it is applied first to accelerate the sequence in x for each value of y and then accelerating in y.

These tables aim at assessing the convergence acceleration performances with respect to the reference Serpent k_{eff}. By inspection of these tables, it should be noticed that the most accurate numerical result, computed by SIMMER with an S_8 scheme and the finest meshes, is closer, within the statistical uncertainty range, to the Monte Carlo calculation than the accelerated ones. In principle, this fact may induce to query the effectiveness of the acceleration algorithm. However, a deeper look at the first column of Table 4 would show an oscillating behaviour of the residual when the S_N order is increased. Therefore, the fact that the finest S_8 calculation is the closest to the reference does not imply that finer angular approximations would provide better results. This non-monotonic behaviour in the angular convergence process, similar to what already observed for the P_N approach in simpler systems (Abrate et al., 2021b,c), could also explain the presence

r	z_4, S_8	W-$\varepsilon(z)$, S_8	W-ε(N), z_4	W-$\varepsilon(z$, N)	W-ε(N, z)
1	787(8)	728(8)	774(8)	722(8)	722(8)
2	79(8)	38(8)	58(8)	28(8)	29(8)
3	46(8)	-28(8)	29(8)	-16(8)	-9(8)
4	2(8)	6(8)	-9(8)	-48(8)	-48(8)
W-$\varepsilon(z$, N, r)			-19(8)		
W-ε(N, z, r)			-11(8)		

Table 6: Distance between the reference $k_{\text{eff,SRP}}$=0.9999(8) and the effective multiplication factor computed by SIMMER and accelerated with the W-ε scheme for the different radial discretisation.

of a residual close to zero in the same table when the double acceleration is applied.

As a general comment, it can be claimed that the acceleration algorithm is quite robust: the residuals show negligible (Tables 4 and 6) or even no change (Table 5) when the order followed to accelerate the different variables changes. It is interesting to notice that, for the entries in Tables 4 to 6 featured by the coarsest frozen parameters (r_1, z_1, S_2) and by the double acceleration, the largest residual is found for the cartesian mesh size r_1. This evidence is justified by the fact that the coarsest x-y mesh poorly represents the flux spatial gradient. However, as visible in Table 6, the k_{eff} converges faster than in the other cases, suggesting that the radial mesh refinement is less important than the other parameters, provided it is adequate to reproduce the geometry accurately enough. This trend is consistent with the fact that in a fast system the neutron mean free path is larger, meaning that a lower spatial resolution can still yield accurate distributions. This is also one of the physical cornerstones lying at the basis of the nodal diffusion method implementation in FRENETIC.

As regards the angular convergence, see Table 4, it seems that most of the error induced by the angular approximation is reduced moving from S_2 to S_6-S_8, assuming that the spatial discretisation residual is negligible after the accelerations in z and r. When the W-ε is consecutively applied to the three variables, the residual becomes very small, around -10 and -20 pcm according to the different acceleration setups. These results suggest that the W-ε scheme seems able to boost the k_{eff} numerical convergence, correcting

the biases due to the angular and spatial approximations. This conjecture would also imply a more subtle yet important consequence, concerning the inherent multi-group approximation error: since most of the residuals are significantly reduced after the spatial and angular extrapolations, it seems that the bias due to the six-group constants is negligible.

The residuals between FRENETIC and SIMMER, available in the Appendix, can be obtained easily, reminding that the difference between Serpent and FRENETIC amounts to 172(8) pcm. Since the z_4 discretisation matches the one adopted in FRENETIC, the analysis of the asymptotic residuals for the cases with this axial mesh provides an estimate of the angular and radial effects. When both N and r are accelerated, the residual between FRENETIC and SIMMER is close to -145 pcm. Since both the few-group data and the axial nodes are the same, this quantity can be interpreted as the asymptotic error induced by using the discrete ordinates approach and a cartesian mesh instead of a nodal diffusion method. This discrepancy is inherently related to the physico-numerical models available in the codes, and depends on the core configuration. Since the CRs insertion emphasizes the transport effects, the off-critical configurations, i.e. the CRs are withdrawn, should be featured by a smaller error. In order to draw more compelling conclusions, the same convergence studies should be performed for different reactor configurations and multi-group datasets, in order to shed some light on the approximation error trend.

5. Conclusions

In this paper, the first steps of the code-to-code comparison between FRENETIC and SIMMER for the simulation of lead-cooled fast reactors were reported. Different options for the geometrical representation of a hexagonal core in SIMMER were compared to the coarse-mesh approach adopted in FRENETIC, which is tailored to hexagonal SAs. Neutronic simulations were performed, carefully ensuring the consistency of the nuclear data fed to the two codes, showing that the FRENETIC diffusion solution is in very good agreement with the SIMMER S_N transport solution. Finally, the W-ε scheme was applied to a set of effective multiplication values computed by SIMMER allowing to extrapolate the asymptotic trend of the different approximation errors. The outcomes of this systematic convergence study indicate that: (i) the quadrature order convergence is non-monotonic; (ii) the numerical convergence associated to the radial mesh is faster than the oth-

ers; (iii) the six-group constants do not seem to introduce a systematic bias on the final results. These considerations have important implications also for FRENETIC: (i), together with the good agreement on the radial power distribution, suggests that the low-order diffusion approximation is adequate to reproduce the full-core macroscopic behaviour; (ii) confirms that a coarse mesh nodal diffusion approach is adequate to correctly retrieve the spatial effects; (iii) suggests the adequateness of the few-group energy grid adopted for the collapsing.

However, contrarily to the systematic study performed on the regions subdivision, the six-group energy grid was chosen according to *ad hoc* considerations regarding the flux spectrum. Therefore, a more thorough study involving the adoption of structured approaches, e.g. based on a genetic algorithm (Massone et al., 2017), is envisaged. In perspective, the natural prosecution of this benchmark activity would be represented by considering the multi-physics NE-TH coupling in both codes, which would allow to further qualify the FRENETIC code for the multiphysics simulation of lead-cooled fast reactors.

Acknowledgements

The authors would like to express their gratitude to Professor Barry D. Ganapol for having disclosed the power and the beauty of the Wynn ε method for reactor physics applications.

Appendix A. 2D code-to-code benchmark

Appendix A.1. ALFRED configuration without neutron absorbers

In the spirit of an increasingly detailed simulation framework aimed at comparing the different reactor modeling options, the ALFRED reactor model is initially simplified by replacing both the CRs and SRs with the surrounding fuel assemblies (FAs), as sketched in Figure A.13. There are three main reasons that justify this modeling choice. First, it allows to obtain a model which could be well represented by the 2D r-z cylindrical geometry available in SIMMER: the SAs are arranged in a set of homogeneous almost-circular rings, see Figure 1, without the CRs and SRs spots that cannot be reliably modeled by means of a cylinder. Second, it allows to simplify the sensitivity analysis concerning the active length subdivision. Indeed, as visible in Figure 5, the flux energy spectrum computed by Serpent shows a non-negligible

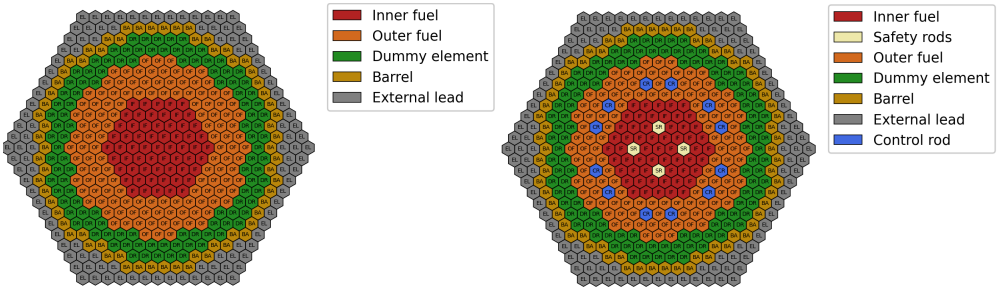

Figure A.13: Radial (x-y plane) sections of the ALFRED 3D model for the few-group constants calculation for the cases without (left) and with (right) control and safety rods.

gradient from the active length edge to the its center, implying possible significant variations in the collapsed few-group data. Finally, removing the strong neutron absorbers, poorly approximated by low-order transport models like diffusion, allows to estimate the impact induced by their presence on the k_{eff} evaluation. Four axial partitions, indicated by the black dashed lines, are presented in Figure A.14. Assuming the origin of the z-axis placed at the active half-height, the α case (top left) presents three axial fuel slices located at -30, -20, +20 and +30 cm, the γ case (bottom left) has a single region between -30 and +30, while the active regions of the β and δ cases (top and bottom right, respectively) are featured by uniformly (-30, -18, -6, +6, +18 and +30) and non-uniformly (-30, -25, -18, +18, +25 and +30 cm) spaced slices, respectively. It noteworthy that the axial slicing is already performed in the multi-group constants generation process, therefore the fuel partition used in the deterministic codes matches the one in Serpent.

Table A.7: Effective multiplication factor computed by FRENETIC (FRN) in 3D and SIMMER (SMR) in 2D for the configuration without control and safety rods. The reference k_{eff} computed by Serpent is 1.13793(4).

	$k_{\text{eff,FRN}}$	$k_{\text{SRP}} - k_{\text{FRN}}$ [pcm]	$k_{\text{SMR,S}_4}$	$k_{\text{SRP}} - k_{\text{SMR}}$ [pcm], S_4	$k_{\text{SMR,S}_8}$	$k_{\text{SRP}} - k_{\text{SMR}}$ [pcm], S_8
α	1.13990	-197	1.14461	-668	1.14410	-617
β	1.13979	-186	1.14450	-657	1.14399	-606
γ	1.14003	-210	1.14469	-676	1.14418	-625
δ	1.13960	-167	1.14418	-625	1.14368	-575

Table A.7 clearly shows a significant bias in the SIMMER k_{eff} results

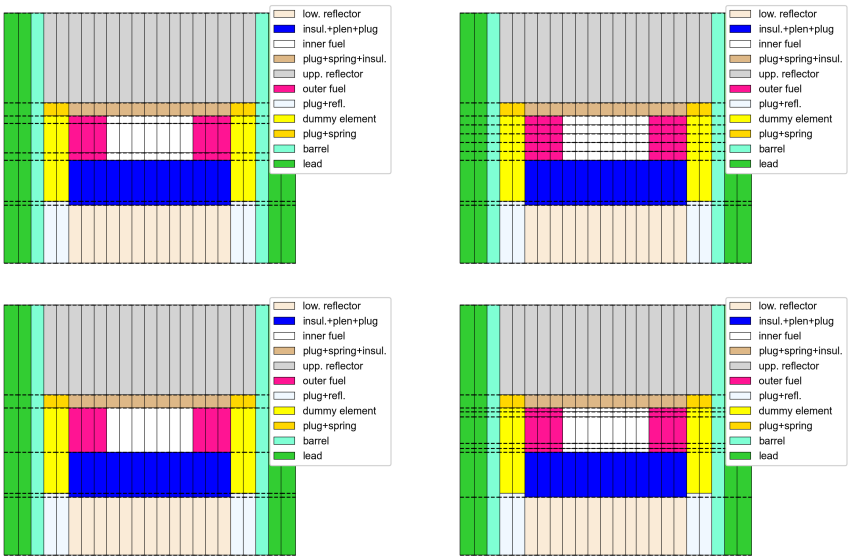

Figure A.14: Cases α (top left), β (top right), γ (bottom left) and δ (bottom right) axial configurations of the ALFRED 3D model without control and safety rods. The partitions of the inner and outer fuel regions employed in both FRENETIC and SIMMER match with the one adopted in Serpent.

with respect to the reference computed by Serpent. The overestimation by SIMMER should be due mostly to geometrical effects, i.e. the 2D cylinder has a lower surface-to-volume ratio compared to the original hexagon-shaped system depicted in Figure 2. In this respect, the 3D nodal diffusion model employed by FRENETIC is definitely more accurate than the discrete ordinates approach applied to an approximated geometry, suggesting that the calculations are sensitive to the spatial shape of the system, consistently with the fact that the neutron distribution in fast system is dominated by leakages rather than local spatial effects. Nonetheless, it is not trivial to identify the specific source of the k_{eff} overestimation with respect to Serpent, due to the competing effects of different models (diffusion vs. transport) and numerical approximations (e.g., the homogenisation and collapsing of the multi-group constants, compensation effects, ...). Concerning the axial partitions, the γ case is the worst one, suggesting that the flux spectrum variation along the SAs axis significantly impacts the collapsing process. Increasing the number of partitions slightly improves the accuracy, but the enhancement is quite limited ($\sim$ 10 pcm) when five subdivisions are adopted instead of three. The

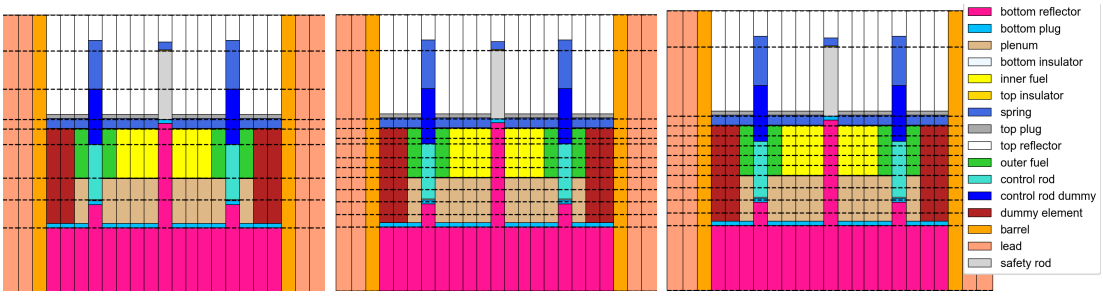

Figure A.15: Case A0 (left), A1 (center) and A2 (right) axial regions subdivision to spatially homogenise the *a posteriori* the few-group data for FRENETIC and SIMMER calculations.

choice yielding the closest results to the reference is the δ model, whose subdivision tries to follow the spectrum gradient in Figure 5. It should be remarked that these observations hold for all the various transport approximations considered.

Appendix A.2. ALFRED nominal configuration

Figure A.15 shows three possible partitions for the post-homogenisation from the the Serpent model off-critical A to the corresponding FRENETIC one. The three models, named A0, A1 and A2, respectively, are featured by the same partitions for the top and bottom regions, but different cuts in the others. The A0 case is the coarsest, while A1 and A2 are finer: they are identical, except for the active length. Starting from the plenum in the FAs, two bins are adopted in the A0 case (left), in order to distinguish the control rod absorber from the bottom reflector, while equally spaced axial bins are adopted in the A1 (center) and A2 (right) cases. Concerning the active length, only one cut is employed in A0 to separate the absorber from the control rod dummy, while more are used in A1 and A2. Contrarily to section Appendix A.1, the inner and outer FAs are axially subdivided in the deterministic codes but not in Serpent, where the few-group data are homogenised over a unique axial bin. The choice of using more bins filled with the same material properties takes into account possible translations of the CRs. It is important to remark here that in A2 the choice of equally spacing the axial segments leads to a bin including both CR absorber and dummy regions, whereas in A1 this does not occur.

The 3D to 2D r-z transition procedure leaves some freedom in the choice of the number of rings and in the positioning of the control and safety rods.

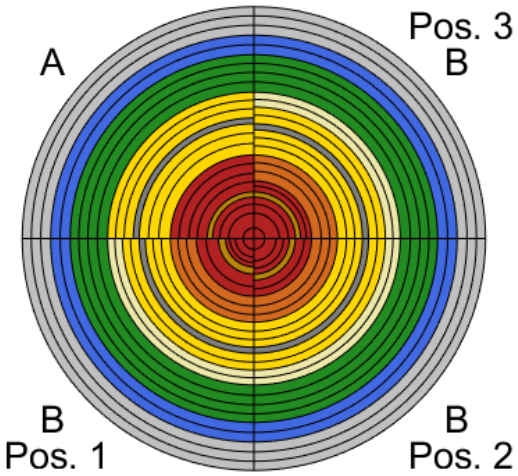

Figure A.16: SIMMER 2D geometrical models.

In fact, the rings which represent them can be placed before or after the ones related to the other SAs with the same distance from the core centre. In order to assess the effect of such choices, we have considered three different positions of the SR rings (referred as Pos. 1 to 3), shown in A.16. The values of k_{eff} calculated by SIMMER for these configurations, based on the B model, are reported in Table A.8; this integral parameter is compared with the corresponding one of the 3D FRENETIC simulation.

Depending on the SR ring position, the multiplication coefficient can change up to 130 pcm, monotonically increasing as the ring is pushed away from the core centre. Considering that the volume of the SR ring is constant, as the number of FAs inside the ring increases, the thickness of the SR ring is reduced, making it more transparent to neutrons: this decreases the perturbation created by the ring, hence raising the flux in the core centre and the multiplication factor consequently.

Therefore, despite the Pos. 3 configuration (with the SR ring very far from the core centre) best approaches the 3D multiplication factor, this does not mean that such case is the optimal representation of the system physics. Nonetheless, the Pos. 3 of the SR has been adopted for the next 2D calculations. Table A.9 shows the k_{eff} computed with the axial cuts presented above.

Table A.8: Comparison among the effective multiplication factors computed by FRENETIC (FRN) in 3D and SIMMER (SMR) in 2D moving the safety rod with respect to the reactor centre. The reference k_{eff} computed by FRENETIC is 0.99818

SR ring position	FAs inside the SR ring	$k_{\text{eff,SMR}}$	$k_{\text{eff,SMR}} - k_{\text{eff,FRN}}$
Pos. 1	7	0.99426	-392
Pos. 2	13	0.99456	-362
Pos. 3	19	0.99552	-266

Concerning FRENETIC, as reasonably expected, increasing the number of regions, and thus the number of axial nodes used in the nodal diffusion, improves ($\sim$ 100 pcm) the agreement from case A0 to A1. However, when the CR absorber and dummy are homogenised in the A2 cases, the difference changes sign and the k_{eff} computed by FRENETIC dramatically approaches the reference value (Serpent). It is clear that this is due to a compensation of the different approximation errors rather than to a better choice of the axial cuts. Indeed, it is pivotal to clarify that here the few-group data are inherently biased by the fact that they are generated with the off-critical Serpent configuration, but they are employed to simulate a close-to-critical configuration in the deterministic codes. This result shows that the axial regions *a posteriori* homogenisation may yield to falsely accurate results, especially when it involves important regions like fuel or poisons. Therefore, performing the region spatial homogenisation directly in Serpent should be a better choice. Regarding SIMMER, in addition to the shape effects, already

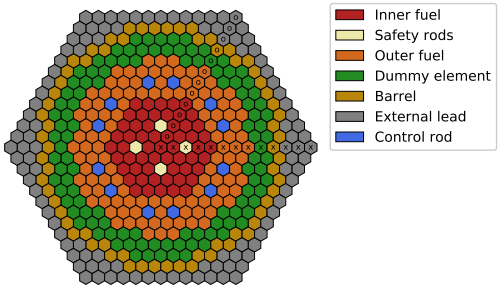

Figure A.17: Radial map of the ALFRED core. The X and O identify the assemblies used in the FRENETIC 3D - SIMMER 2D comparison.

addressed in section Appendix A.1, the ring arrangement of the CRs and SRs increases the bias with respect to the reference case with respect to the

model without absorbers. It is interesting to notice that, unlike FRENETIC simulations, the A2 model in SIMMER yields the worst results, suggesting once again that there are some complications related to different modelling approximations.

Table A.9: Effective multiplication factor computed by FRENETIC (FRN) in 3D and SIMMER (SMR) in 2D, S_4, post-homogenising the few-group data generated by Serpent (SRP) according to some possible axial subdivisions. The reference k_{eff} computed by Serpent is 0.9999(8).

	$k_{\text{eff,FRN}}$	$k_{\text{eff,SRP}} - k_{\text{eff,FRN}}$ [pcm]	$k_{\text{eff,SRP}}$	$k_{\text{eff,SRP}} - k_{\text{eff,SMR}}$ [pcm]
A0	0.993002	696.4	1.010632	-1066.6
A1	0.993922	604.4	1.009576	-961
A2	1.000455	-48.4	1.015290	-1532

As already explained, the calculations discussed so far have been performed with the data generated with the off-critical A Serpent model. In order to quantify the impact of the data collapsed with the close-to-critical spectrum on k_{eff}, some additional cases have been addressed in Table A.10. The bias induced by the two data-sets is consistent between FRENETIC and SIMMER for the 3D case and quite significant, with $\sim$ 400 pcm. For the SIMMER 2D case the impact due to the two data-sets is much lower, likely due to a compensation with the geometrical approximations involving the reactor and the absorbers.

Table A.10: Effective multiplication factor computed with two sets of few-group constants for the ALFRED A version with the CRs inserted. The sets are generated with the off-critical (OC) and close-to-critical (CC) A Serpent models, respectively.

	FRENETIC	SIMMER, (2D, S_8)	SIMMER, (3D, S_8)
$k_{\text{eff,OC}}$	0.993922	1.009576	0.992450
$k_{\text{eff,CC}}$	0.997656	1.011380	0.996270
$\Delta k_{\text{eff,OC-CC}}$ [pcm]	-373.4	-180.4	-381.9

For the two sets of assemblies indicated with an "X" and "O" in the FRENETIC 3D model (Figure A.17), Figure A.18 shows the group-wise flux computed by SIMMER and FRENETIC using the A0 partition (see again Figure A.15 for reference). It can be seen that the effect of the refinement of axial sub-partitions in SIMMER is negligible, and that, as expected, the results of the 2D SIMMER model are more representative of the "X" set of

bars. Results for the A1 and A2 partitions are similar to A0 and therefore are not reported.

Figure A.19 shows the group-wise flux computed by SIMMER and FRENETIC using nuclear data according to the B1 region subdivision model, showing a similar behavior with respect to the one observed for the A0 case.

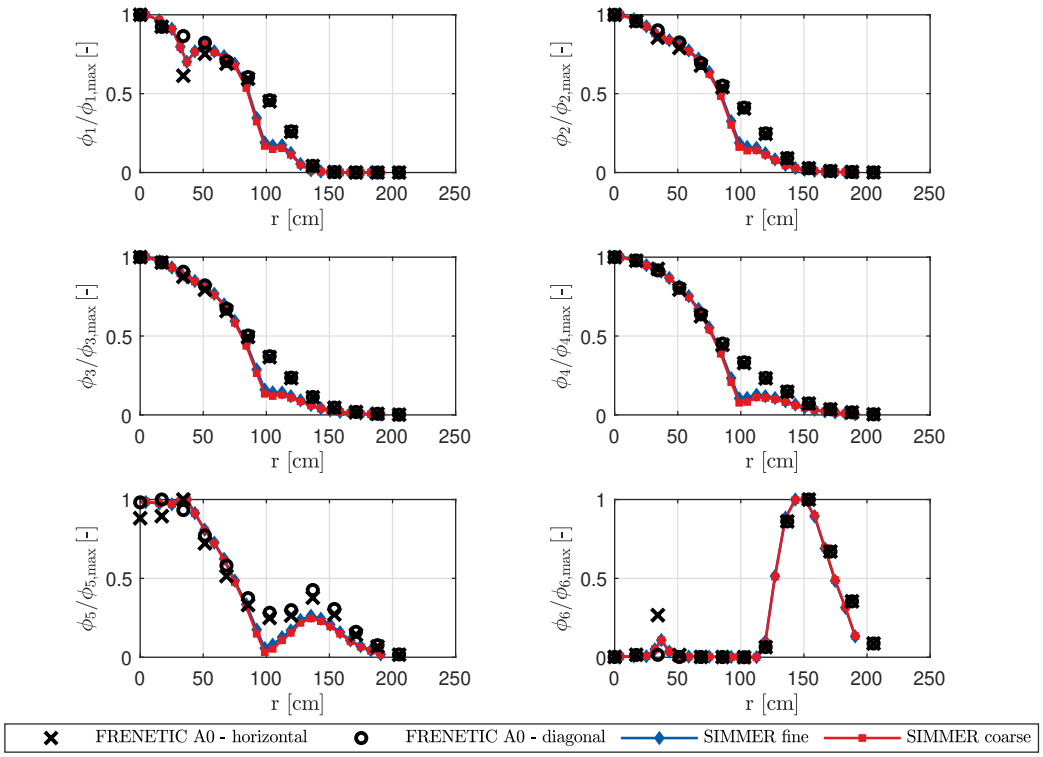

Figure A.18: Assembly-wise, six-group flux traverses for the case A0 compared with 2D SIMMER results.

Appendix B. Wynn-ε acceleration scheme

In the following, the residuals between the accelerated SIMMER sequences and the effective multiplication factor computed by FRENETIC are reported.

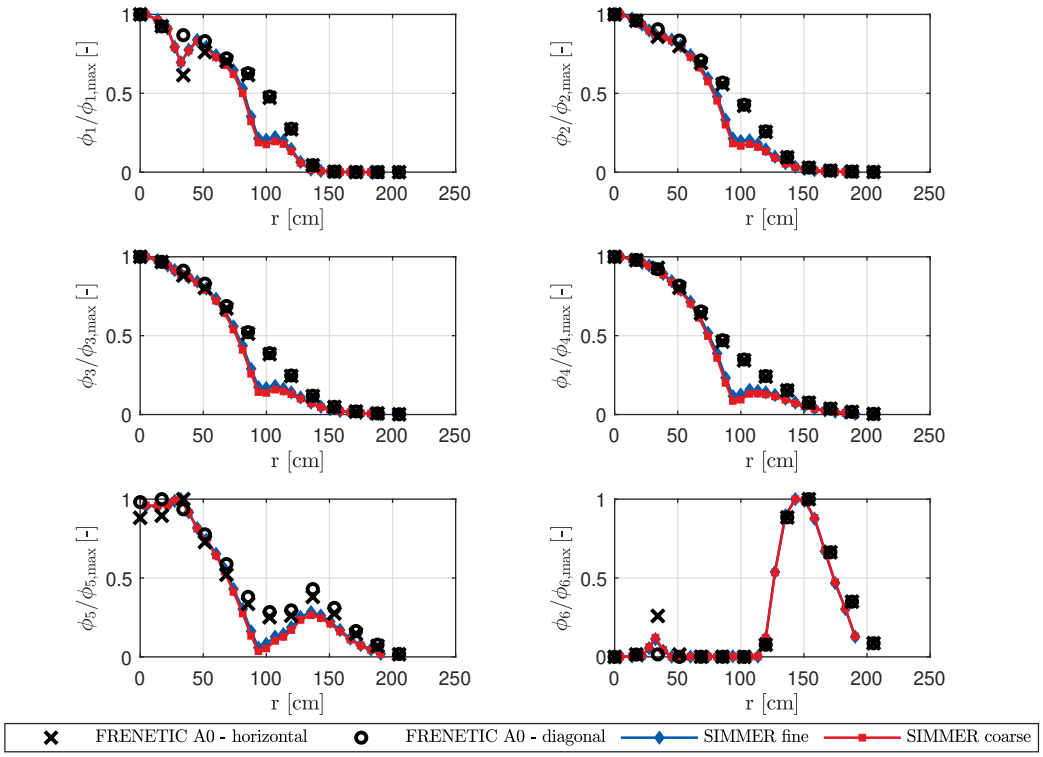

Figure A.19: Assembly-wise, six-group flux traverses for the case B1 compared with 2D SIMMER results.

N	r_4, z_4	W-$\varepsilon(r)$, z_4	W-$\varepsilon(z)$, r_4	W-$\varepsilon(r, z)$	W-$\varepsilon(z, r)$
2	113	152	89	18	-10
4	-207	-180	-261	-252	-260
6	-179	-139	-214	-172	-172
8	-169	-127	-166	-204	-206
W-$\varepsilon(r, z,$ N)			-191		
W-$\varepsilon(z, r,$ N)			-195		

Table B.11: Distance between FRENETIC ($k_{\text{eff,FRN}}$=0.99818) and the effective multiplication factor computed by SIMMER and accelerated with the W-ε scheme for the different discrete ordinates order.

z	r_4, S_8	W-$\varepsilon(r)$, S_8	W-ε(N), r_4	W-$\varepsilon(r,$ N)	W-ε(N, r)
1	54	109	35	89	88
2	-85	-32	-98	-48	-48
3	-136	-110	-161	-116	-116
4	-170	-127	-181	-144	-143
W-$\varepsilon(r,$ N, $z)$			-182		
W-ε(N, r, $z)$			-183		

Table B.12: Distance between FRENETIC ($k_{\text{eff,FRN}}$=0.99818) and the effective multiplication factor computed by SIMMER and accelerated with the W-ε scheme for the different axial discretisations.

r	z_4, S_8	W-$\varepsilon(z)$, S_8	W-ε(N), z_4	W-$\varepsilon(z$, N)	W-ε(N, z)
1	615	556	774(8)	550	550
2	-93	-133	58(8)	-144	-142
3	-126	-200	29(8)	-188	-181
4	-170	-166	-9(8)	-220	-220
W-$\varepsilon(z$, N, $r)$			-191		
W-ε(N, z, $r)$			-183		

Table B.13: Distance between FRENETIC ($k_{\text{eff,FRN}}$=0.99818) and the effective multiplication factor computed by SIMMER and accelerated with the W-ε scheme for the different radial discretisations.

References

D. Caron, R. Bonifetto, S. Dulla, V. Mascolino, P. Ravetto, L. Savoldi, D. Valerio, R. Zanino, Full-core coupled neutronic/thermal-hydraulic modelling of the EBR-II SHRT-45R transient, International Journal of Energy Research 42 (2018) 134–150. URL: http://doi.wiley.com/10.1002/er.3571. doi:doi:10.1002/er.3571.

R. Zanino, R. Bonifetto, L. Richard, A. Del Nevo, Benchmark and preliminary validation of the thermal-hydraulic module of the FRENETIC code against EBR-II data, Embedded Topical Meeting on Advances in Thermal Hydraulics, ATH 2014, Held at the American Nuclear Society 2014 Annual Meeting (2014) 173–187.

G. F. Nallo, N. Abrate, S. Dulla, P. Ravetto, D. Valerio, Neutronic benchmark of the FRENETIC code for the multiphysics analysis of lead fast reactors, The European Physical Journal Plus 135 (2020) 238. URL: https://doi.org/10.1140/epjp/s13360-020-00171-8. doi:doi:10.1140/epjp/s13360-020-00171-8.

J. Leppänen, M. Pusa, T. Viitanen, V. Valtavirta, T. Kaltiaisenaho, The Serpent Monte Carlo code: Status, development and applications in 2013, Annals of Nuclear Energy 82 (2015) 142–150. doi:doi:10.1016/j.anucene.2014.08.024.

W. L. Oberkampf, T. G. Trucano, M. M. Pilch, Predictive Capability Maturity Model for computational modeling and simulation., Technical Report, Sandia National Laboratories (SNL), Albuquerque, NM, and Livermore, CA (United States), 2007. URL: https://www.osti.gov/biblio/976951. doi:doi:10.2172/976951.

S. Kondo, H. Yamano, T. Suzuki, SIMMER-III: A computer program for LMFR core disruptive accident analysis. Version 2. H model summary and program description, 2000. URL: https://inis.iaea.org/search/search.aspx?orig_q=RN:33004688.

W. Maschek, A. Rineiski, M. Flad, P. Liu, X. Chen, Y. Tobita, H. Yamano, T. Suzuki, S. Fujita, K. Kamiyama, S. Pigny, T. Cadiou, K. Morita, G. Bandini, The SIMMER safety code system and its validation efforts for fast reactor application, in: International Conference on the Physics of Reactors 2008, PHYSOR 08, International Conference on the Physics of Reactors 2008, PHYSOR 08, Paul Scherrer Institut, 2008, pp. 2370–2378.

G. Grasso, C. Petrovich, D. Mattioli, C. Artioli, P. Sciora, D. Gugiu, G. Bandini, E. Bubelis, K. Mikityuk, The core design of ALFRED, a demonstrator for

the European lead-cooled reactors, Nuclear Engineering and Design 278 (2014) 287–301.

M. Massone, F. Gabrielli, A. Rineiski, A genetic algorithm for multigroup energy structure search, Annals of Nuclear Energy 105 (2017) 369–387. doi:doi:10.1016/j.anucene.2017.03.022.

R. Bonifetto, S. Dulla, P. Ravetto, L. S. Richard, R. Zanino, A full-core coupled neutronic/thermal-hydraulic code for the modeling of lead-cooled nuclear fast reactors, Nuclear Engineering and Design 261 (2013) 85–94. URL: https://www.sciencedirect.com/science/article/pii/S0029549313001726. doi:doi:10.1016/J.NUCENGDES.2013.03.030.

D. Caron, S. Dulla, P. Ravetto, New aspects in the implementation of the quasi-static method for the solution of neutron diffusion problems in the framework of a nodal method, Annals of Nuclear Energy 87 (2016) 34–48. URL: https://www.sciencedirect.com/science/article/pii/S0306454915001127. doi:doi:https://doi.org/10.1016/j.anucene.2015.02.035, special Issue of The 3rd International Conference on Physics and Technology of Reactors and Application.

R. Zanino, R. Bonifetto, A. Ciampichetti, I. Di Piazza, L. Savoldi Richard, M. Tarantino, First validation of the FRENETIC code thermal-hydraulic model against the ENEA integral circulation experiment, Transactions of the American Nuclear Society 107 (2012) 1395–1398.

R. Zanino, R. Bonifetto, A. Del Nevo, L. Savoldi Richard, Benchmark and preliminary validation of the thermal-hydraulic module of the FRENETIC code against EBR-II data, in: Embedded Topical Meeting on Advances in Thermal Hydraulics, ATH 2014, Held at the American Nuclear Society 2014 Annual Meeting, 2014.

W. R. Bohl, L. B. Luck, SIMMER-II: A Computer Program for LMFBR Disrupted Core Analysis, Technical Report, Los Alamos National Lab. (LANL), Los Alamos, New Mexico (United States), 1990.

H. Yamano, S. Fujita, Y. Tobita, I. Sato, H. Niwa, Development of a three-dimensional CDA analysis code: SIMMER-IV and its first application to reactor case, Nucl. Eng. Des. 238 (2008) 66–73.

Y. Tobita, S. Kondo, H. Yamano, K. Morita, W. Maschek, P. Coste, T. Cadiou, The development of simmer-iii, an advanced computer program for lmfr safety

analysis, and its application to sodium experiments, Nuclear Technology 153 (2006a) 245–255. URL: https://doi.org/10.13182/NT06-2. doi:doi:10.13182/NT06-2. arXiv:https://doi.org/10.13182/NT06-2.

Y. Tobita, S. Kondo, H. Yamano, K. Morita, W. Maschek, P. Coste, T. Cadiou, The Development of SIMMER-III, An Advanced Computer Program for LMFR Safety Analysis, and Its Application to Sodium Experiments, Nuclear Technology 153 (2006b) 245–255. URL: https://doi.org/10.13182/NT06-2. doi:doi:10.13182/NT06-2. arXiv:https://doi.org/10.13182/NT06-2.

S. Wang, A. Rineiski, W. Maschek, Molten salt related extensions of the SIMMER-III code and its application for a burner reactor, Nuclear Engineering and Design 236 (2006) 1580–1588. URL: https://www.sciencedirect.com/science/article/pii/S002954930600330X. doi:doi:https://doi.org/10.1016/j.nucengdes.2006.04.022, 13th International Conference on Nuclear Energy.

R. E. Alcouffe, R. S. Baker, F. W. Brinkley, D. R. Marr, R. D. O'Dell, W. F. Walters, DANTSYS: A diffusion accelerated neutral particle transport code system, Technical Report, Los Alamos National Lab. (LANL), Los Alamos, New Mexico (United States), 1995. URL: https://www.osti.gov/biblio/212580. doi:doi:10.2172/212580.

I. Bondarenko, Group constants for nuclear reactor calculations, Consultants Bureau, New York, 1964.

M. Folk, G. Heber, Q. Koziol, E. Pourmal, D. Robinson, An overview of the hdf5 technology suite and its applications, in: Proceedings of the EDBT/ICDT 2011 Workshop on Array Databases, AD '11, Association for Computing Machinery, New York, NY, USA, 2011, p. 36–47. URL: https://doi.org/10.1145/1966895.1966900. doi:doi:10.1145/1966895.1966900.

A. E. Johnson, D. Kotlyar, S. Terlizzi, G. Ridley, serpentTools: A Python package for expediting analysis with Serpent, Nuclear Science and Engineering 194 (2020) 1016–1024. URL: https://doi.org/10.1080/00295639.2020.1723992. doi:doi:10.1080/00295639.2020.1723992. arXiv:https://doi.org/10.1080/00295639.2020.1723992.

D. Brown, M. Chadwick, R. Capote, A. Kahler, A. Trkov, M. Herman, A. Sonzogni, Y. Danon, A. Carlson, M. Dunn, D. Smith, G. Hale, G. Arbanas, R. Arcilla, C. Bates, B. Beck, B. Becker, F. Brown, R. Casperson, J. Conlin, D. Cullen, M.-A. Descalle, R. Firestone, T. Gaines, K. Guber, A. Hawari, J. Holmes, T. Johnson, T. Kawano, B. Kiedrowski, A. Koning,

S. Kopecky, L. Leal, J. Lestone, C. Lubitz, J. Márquez Damián, C. Mattoon, E. McCutchan, S. Mughabghab, P. Navratil, D. Neudecker, G. Nobre, G. Noguere, M. Paris, M. Pigni, A. Plompen, B. Pritychenko, V. Pronyaev, D. Roubtsov, D. Rochman, P. Romano, P. Schillebeeckx, S. Simakov, M. Sin, I. Sirakov, B. Sleaford, V. Sobes, E. Soukhovitskii, I. Stetcu, P. Talou, I. Thompson, S. van der Marck, L. Welser-Sherrill, D. Wiarda, M. White, J. Wormald, R. Wright, M. Zerkle, G. Žerovnik, Y. Zhu, ENDF/B-VIII.0: The 8th major release of the nuclear reaction data library with CIELO-project cross sections, new standards and thermal scattering data, Nuclear Data Sheets 148 (2018) 1 – 142. URL: http://www.sciencedirect.com/science/article/pii/S0090375218300206. doi:doi:https://doi.org/10.1016/j.nds.2018.02.001, special Issue on Nuclear Reaction Data.

M. Marchetti, Neutronics Methods for Transient and Safety Analysis of Fast Reactors, KIT Scientific Publishing, Karlsruhe, 2017. doi:doi:10.5445/KSP/1000063691.

P. Wynn, On a device for computing the em(Sn) transformation, Math. Tables Aids Comput. 10 (1956) 91–96.

B. Ganapol, More than you wanted to know about convergence acceleration, in: Radiation Protection and Shielding Division Workshop (ANS), Knoxville, TN, 2014.

D. Shanks, Nonlinear transformations of divergent and slowly convergent sequences, J. Math. Phys. 34 (1955) 1–42.

Fredrik Johansson, mpmath: a Python library for arbitrary-precision floating-point arithmetic, 2017. URL: https://doi.org/10.5281/zenodo.1476882. doi:doi:10.5281/zenodo.1476882.

N. Abrate, B. Ganapol, S. Dulla, P. Ravetto, P. Saracco, A. Zoia, Convergence Acceleration Aspects in the Solution of the P_N Neutron Transport Eigenvalue Problem, in: International M&C Conference 2021, Rayleigh (North Carolina, U.S.A.), 2021a.

N. Abrate, M. Burrone, S. Dulla, P. Ravetto, P. Saracco, Eigenvalue formulations for the pn approximation to the neutron transport equation, Journal of Computational and Theoretical Transport 50 (2021b) 407–429. URL: https://doi.org/10.1080/23324309.2020.1856879. doi:doi:10.1080/23324309.2020.1856879. arXiv:https://doi.org/10.1080/23324309.2020.1856879.

N. Abrate, S. Dulla, P. Ravetto, P. Saracco, On some features of the eigenvalue problem for the P_N approximation of the neutron transport equation, Annals of Nuclear Energy 163 (2021c) 108477. URL: https://www.sciencedirect.com/science/article/pii/S0306454921003534. doi:doi:https://doi.org/10.1016/j.anucene.2021.108477.

M. Massone, F. Gabrielli, A. Rineiski, Simmer extension for multi-group energy structure search using genetic algorithm with different fitness functions, Nuclear Engineering and Technology 49 (2017) 1250–1258. URL: https://www.sciencedirect.com/science/article/pii/S173857331730270X. doi:doi:https://doi.org/10.1016/j.net.2017.07.012, special Issue on International Conference on Mathematics and Computational Methods Applied to Nuclear Science and Engineering 2017 (M&C 2017).